Journal of ELECTRONIC MATERIALS, Vol. 43, No. 4, 2014
DOI: 10.1007/s11664-013-2971-7
© 2014 The Author(s). This article is published with open access at Springerlink.com

Suitable Thicknesses of Base Metal and Interlayer, and Evolution of Phases for Ag/Sn/Ag Transient liquid-phase Joints Used for Power Die Attachment

J.F. LI,[1,2] P.A. AGYAKWA,[1] and C.M. JOHNSON[1]

1.—Department of Electrical and Electronic Engineering, The University of Nottingham, University Park, Nottingham NG7 2RD, UK. 2.—e-mail: Jianfeng.Li@nottingham.ac.uk

Real Si insulated gate bipolar transistors with conventional Ni/Ag metallization and dummy Si chips with thickened Ni/Ag metallization have both been bonded, at 250°C for 0 min, 40 min, and 640 min, to Ag foil electroplated with 2.7 μm and 6.8 μm thick Sn as an interlayer. On the basis of characterization of the microstructure of the resulting joints, suitable thicknesses are suggested for the Ag base metal and the Sn interlayer for Ag/Sn/Ag transient liquid-phase (TLP) joints used for power die attachment. The diffusivities of Ag and Sn in the ζAg phase were also obtained. In combination with the kinetic constants of Ag_3Sn growth and diffusivities of Ag and Sn in Ag reported in the literature, the diffusivities of Ag and Sn in the ζAg phase were also used to simulate and predict diffusion-controlled growth and evolution of the phases in Ag/Sn/Ag TLP joints during extended bonding and in service.

Key words: Transient liquid-phase (TLP) bonding, die attachment, diffusion, interfacial reaction, intermetallic compounds, solid solution

INTRODUCTION

Transient liquid-phase (TLP) bonding used in electronic packaging and interconnects is promising alternative joining technology for high-temperature and high-power-density power electronics.[1–4] This is because such TLP joints can formed by use of a lower-melting-point Sn or In interlayer which reacts with and/or diffuses into a surrounding base metal during extended isothermal solidification. TLP bonding can, hence, be performed at relatively low temperatures similar to those used for conventional soldering yet result in higher remelt temperatures of the joints produced.[4] Therefore, TLP joints are expected to be more creep-resistant and more reliable than conventional Sn-based solder joints for applications at elevated temperatures.

As reported in two previous papers on electronic packaging and interconnects[5,6], use of TLP bonding to join the base metals Ag, Au, and Cu has been extensively investigated,[3–13] and joining of the base metals Ni, Pd, Pt, and Zr has also been reported.[14–16] When acceptable bonding temperatures and times are used, the TLP joints produced generally consist of intermetallic compounds (IMCs) of the base metals and the Sn, In, InSn, SnBi, $BiIn_2$, or SnInBi interlayer. Although the IMCs are more brittle than the corresponding base metals, they have much higher mechanical strength and creep resistance than the conventional Sn-based solders used in electronic packaging and interconnects. Indeed, significantly improved reliability of the TLP joint consisting of Cu_6Sn_5 and Cu_3Sn IMCs used to attach 1200 V and 150 A Si insulated gate bipolar transistors (IGBTs) to ceramic-based substrates was demonstrated by means of an active power cycling experiment at maximum junction temperatures of 165–171°C.[17]

This paper is concerned with the Ag/Sn/Ag TLP system for which the sequence of formation and evolution of the intermetallic phases can be predicted by use of the binary Ag–Sn phase diagram shown in Fig. 1.[18]

The feasibility of using this system for joining components for use in the high-temperature electronics industry was proved in the late 1980s.[4,7] In

(Received February 22, 2013; accepted December 30, 2013; published online January 22, 2014)

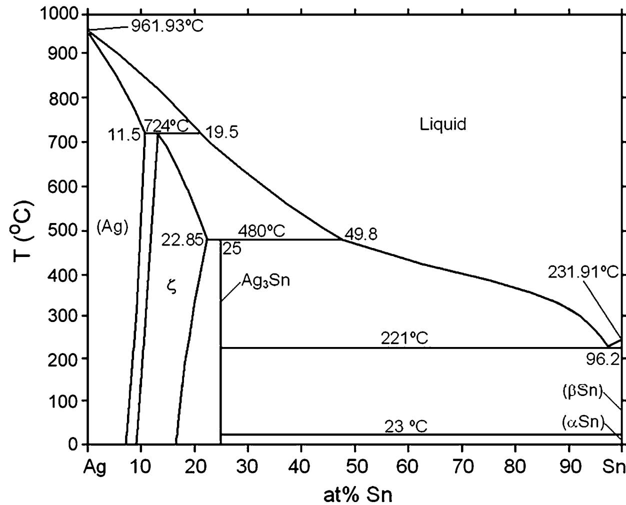

Fig. 1. Phase diagram of the binary Ag–Sn system.

previous work,[5] the thickening kinetics of Ag_3Sn IMC growth was investigated by sandwiching a thin layer of Sn between two pieces of Ag foil at 260°C, 300°C, and 340°C. In the work reported in this paper, both real Si IGBTs with conventional Ni/Ag metallization and dummy Si chips with thickened Ni/Ag metallization have been bonded, at 250°C for 0 min, 40 min, and 640 min, to Ag foil electroplated with 2.7 μm and 6.8 μm thick Sn as interlayer. Such features as the microstructure of the phases, voids, and thicknesses of the resulting joints were then characterized and analyzed. The objectives of this work were:

1. to determine suitable thicknesses of interlayer Sn and base metal Ag on both the power die and the supporting substrate for an Ag/Sn/Ag TLP system which can be used in power die attachment;
2. to obtain and report the diffusivities of Ag and Sn in ξAg IMC, which are not available in the literature; and
3. to simulate the diffusion-controlled growth and evolution of phases in Ag/Sn/Ag TLP joints during extended bonding, to enable prediction of the phases stably existing in Ag/Sn/Ag TLP joints in service.

Given that conventional Sn-based solder joints are not usually reliable at temperatures above 125°C, the results obtained in this work will be useful for utilization of Ag/Sn/Ag TLP joints in the development and manufacture of high-temperature power electronic systems. For instance, it is desirable to develop power electronics modules which are reliable in continuous operation at an ambient temperature of 150°C and above for periods of several years. Examples includes aerospace, in which there is increasing use of electronic rather than hydraulic or pneumatic systems, automotive underhood applications in conventional, hybrid, and electric drive systems, and down-hole gas and oil field applications. Ag/Sn/Ag TLP joints are well suited to these applications and are even able to operate at temperatures higher than the processing temperature.

EXPERIMENTAL

Preparation of Samples

The real Si IGBTs used in this work were 13 mm × 13 mm × 0.3 mm in size with conventional 0.8/0.7 μm thick Ni/Ag metallization. The dummy Si chips were 13 mm × 13 mm × 1 mm Si chips with thickened (i.e. 1/6 μm) Ni/Ag metallization deposited by sputtering. Both were obtained from Dynex Semiconductor (Lincoln, UK). Their cross-sectional scanning electronic microscopy (SEM) images are shown in Fig. 2. The as-received Ag foil electroplated with Sn 2.7 μm and 3.1 μm or 6.8 μm and 7.5 μm thick on both sides were discs 100 mm in diameter; the Ag was 100 μm thick. These were obtained from Applied Materials Technology (Lincoln, UK). Their cross-sectional SEM images are given in Fig. 3.

All the samples were prepared by use of the sample configuration and temperature–pressure profile illustrated schematically in Fig. 4. The as-received Ag discs plated with the Sn layers were first cut into 13 mm × 13 mm pieces. A real Si IGBT (or a dummy Si chip) was then placed in contact with the surface of a 13 mm × 13 mm piece of Ag foil plated with 2.7 μm thick Sn, and another real IGBT (or another dummy Si chip) was placed in contact with the surface of another 13 mm × 13 mm piece of Ag foil plated with 6.8 μm thick Sn. Next, they were brought together, and placed in a house-made bonding rig, where they were inserted into two ∅55 mm × 5 mm Al discs to improve the uniformity of heat delivered from both the top and bottom electric cartridge heaters during the final bonding process. A pressure of ~2 MPa was then applied to the bonding area, and the samples were purged with nitrogen gas (760 mL/min at 1.5 bar). The bonding process was started by subjecting the samples to a temperature profile which involved first heating to 200°C at 45°/min, then heating to 250°C at 25°/min, easily achieved by use of the bonding rig, before holding at 250°C for 0 min, 40 min, or 640 min. Finally, the pressure was released and the samples were removed from the bonding rig when it had cooled to 100°C (after approximately 10 min).

The combinations of Si chips, Ag foil, and dwell time used during the bonding process described above, with their sample codes, are listed in Table I. The focus of this work was the interfacial reactions and microstructures in the Ni/Ag/Sn/Ag and Ag/Sn/Ag/Ni parts of the bonding structure shown in Fig. 4a. The results obtained will be used to determine suitable thicknesses of interlayer Sn and base metal Ag on both the power die and the supporting substrate for Ag/Sn/Ag TLP systems which can be

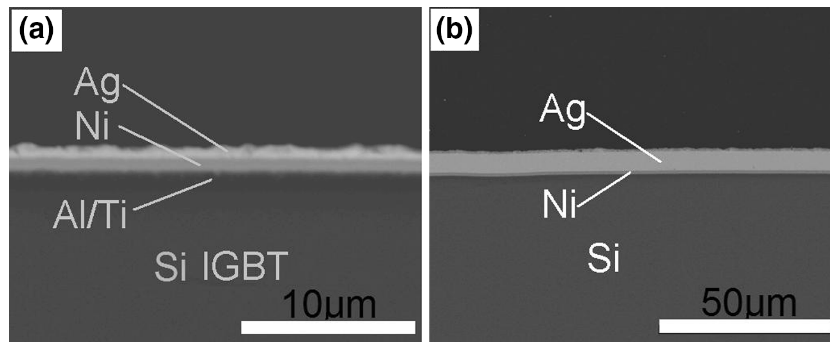

Fig. 2. SEM images of polished cross sections of: (a) real IGBT with conventional Ni/Ag metallization; (b) dummy Si chip with thickened Ni/Ag metallization.

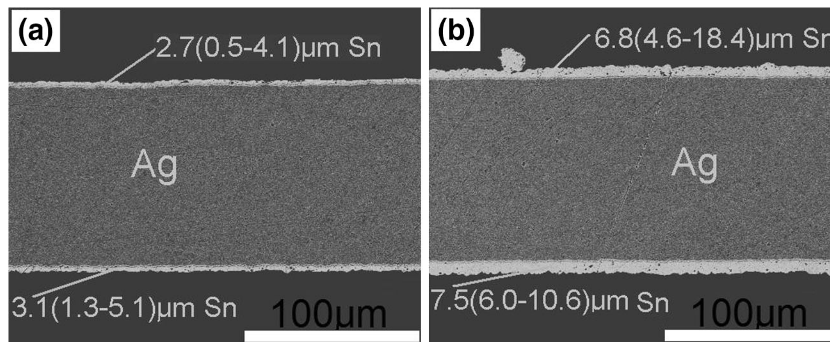

Fig. 3. SEM images of polished cross sections of 100 μm thick Ag foil electroplated with: (a) 2.7 μm thick Sn; (b) 6.8 μm thick Sn.

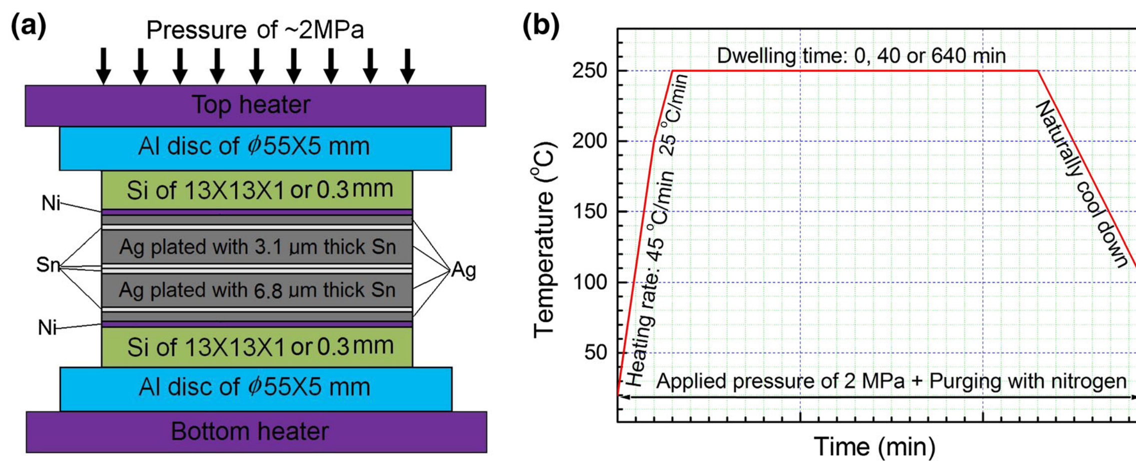

Fig. 4. Schematic illustration of (a) the sample geometry and (b) the temperature–pressure profile used to join both real Si IGBTs and dummy Si chips to Ag foil electroplated with 2.7 μm and 6.8 μm thick Sn. Note that the dimensions of the different components are not to scale.

used for power die attachment. It should be pointed out that some Sn was observed to squeeze out of the bonding areas for all the real Si IGBTs and dummy Si chips bonded to Ag foil plated with 6.8 μm thick Sn. However, no appreciable amount of Sn could be observed outside the bonding areas for all the real Si IGBTs and dummy Si chips bonded to Ag foil plated with 2.7 μm thick Sn.

Metallographic cross-sections of all the bonded samples listed in Table I were prepared for characterization of the microstructure and measurement of the thickness of the IMCs formed. The samples

Table I. Sample codes and the corresponding Si chips, Ag foil, and dwell times used during the bonding process

Code	Thickness of Ag on Si chips (μm)	Thickness of Sn on Ag foil (μm)	Dwell time (min)
A0	0.7	2.7	0
A1	0.7	2.7	40
A2	0.7	2.7	640
B0	0.7	6.8	0
B1	0.7	6.8	40
B2	0.7	6.8	640
C1	6.0	2.7	40
C2	6.0	2.7	640
D1	6.0	6.8	40
D2	6.0	6.8	640

were first mounted in epoxy resin that was cured at room temperature for 24 h. The mounted samples were then successively ground with 800, 1000, and 1200 grit SiC paper and finally polished by use of 3 μm and 1 μm diamond slurries, both for 10 min.

Characterization and Thickness Measurement of IMCs

A JEOL (Tokyo, Japan) 6400 SEM with a back-scattered electron signal was used for imaging and analysis of features of the microstructure. The IMCs formed in the bonded samples were identified by use of an Oxford Instruments (Oxfordshire, UK) ISIS energy-dispersive x-ray spectroscopy (EDXS) micro-analysis system fitted on the SEM. Because it was difficult to determine, from the SEM images, the interface between the Ag_3Sn and the ξAg IMCs, even if both were formed in some of the bonded samples, the total thicknesses of the Ag_3Sn and the ξAg IMCs formed in all the bonded samples, and the thicknesses of the Ni_3Sn_4 IMC formed in the samples obtained by attaching real IGBTs, were measured by use of an image-analysis method described elsewhere.[5,6] The image analysis was performed by use of Image Processing Toolbox Version 5.0.0 of Matlab R14SP2 (The Mathworks, Cambridge, UK). For each sample, three images 512 × 416 pixels in resolution, one 200 μm × 160 μm and two 40 μm × 32 μm in size, were used. A data series for the thickness of each layer in a sample was obtained from 512 × 3 = 1536 intercepted lengths in the through-thickness direction. The resulting thicknesses are reported as mean, standard deviation (SD), and minimum and maximum values.

To measure the individual thicknesses of Ag_3Sn and ξAg IMCs formed in some of the bonded sample, to obtain the diffusivities of Ag and Sn in ξAg IMC, focused ion beam (FIB) ion channeling was used to observe the grain morphology, size, and boundaries of the IMCs formed in samples C1 and C2. This was achieved by using the FEI Quanta200 3D Dual-Beam FIB/SEM (FEI, Europe NanoPort, Achtseweg Noord 5, 5651 GG Eindhoven, The Netherlands) to progressively mill the polished cross sections, which resulted in grain and grain boundary contrast.

RESULTS

Real Si IGBTs with Conventional Ni/Ag Metallization

The microstructure features of real Si IGBTs bonded to Ag foil plated with 2.7 μm thick Sn and those of real Si IGBTs bonded to Ag foil plated with 6.8 μm thick Sn were not noticeably different. Figure 5 shows the SEM images of three samples of real IGBTs bonded to Ag foil plated with 2.7 μm thick Sn. Ag–Sn IMCs could be observed on the Ag foil side only, and, for all the three samples, the Ni barrier layer beneath the upper Ag metallization of the real IGBTs had fully reacted with Sn, forming Ni_3Sn_4. This is quite unusual and will be discussed in more detail below ("Discussion" section).

For sample A0, bonded at 250°C for 0 min, only Ag_3Sn IMC could be detected by EDXS on the Ag foil side. A trace of Sn remained; this was mixed with the Ni_3Sn_4 IMC formed on the IGBT side. For sample, A1 bonded at 250°C for 40 min, both Ag_3Sn and ζAg IMCs were identified by EDXS on the Ag foil side. EDXS revealed that the Ag_3Sn IMC dominated the thickness of the Ag–Sn IMCs, but the interface between the Ag_3Sn and ζAg IMCs was hard to distinguish in the SEM image. Although no appreciable amount of pure Sn remained on the IGBT side, a chain of voids several microns in size was observed along the interface of the Ni_3Sn_4 IMC in contact with the Ag_3Sn IMC on the Ag foil side. For sample A2 bonded at 250°C for 640 min, only ζAg IMC was left on the Ag foil side. The Ni_3Sn_4 IMC and a chain of voids several microns in size formed on the IGBT side were both similar to those observed for sample A1 bonded at 250°C for 40 min.

The total thicknesses measured by image analysis for the Ag–Sn IMCs formed in all the bonded samples are listed in Table II. The means, standard deviations, and maximum values for samples A0 to A2 are almost the same as those for samples B0 to B2, respectively. The mean thicknesses are similar for samples A0, A1, B0, and B1. This may be attributed to the Sn partially squeezed from the bonding areas of samples B0 and B1, which were bonded to Ag foil plated with thicker Sn. On the

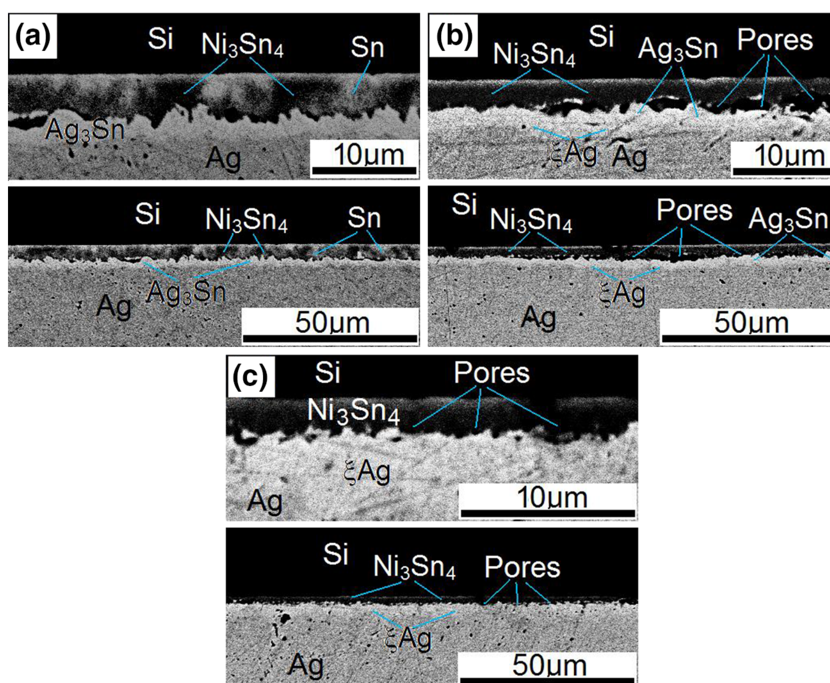

Fig. 5. SEM images of polished cross sections of real Si IGBTs with conventional Ni/Ag metallization on 100 μm thick Ag foil electroplated with 2.7 μm thick Sn at 250°C and 2 MPa: (a) sample A0, 0 min; (b) sample A1, 40 min; (c) sample A2, 640 min.

Table II. Results from measurement, by use of the image-analysis method, of the thickness of the total Ag–Sn IMCs formed in all the bonded samples

Code	Mean (μm)	SD (μm)	Min (μm)	Max (μm)	Ag–Sn IMCs
A0	2.2	0.6	0.7	4.4	Ag_3Sn
A1	2.0	0.4	0.7	3.2	Ag_3Sn + ζAg
A2	3.6	0.6	2.3	5.1	ζAg
B0	2.0	0.6	0.5	3.8	Ag_3Sn
B1	1.7	0.4	0.2	3.2	Ag_3Sn + ζAg
B2	3.8	0.6	2.3	5.5	ζAg
C1	9.9	0.6	8.3	12.0	Ag_3Sn + ζAg
C2	13.5	0.7	12.1	15.1	ζAg
D1	11.2	1.0	7.4	13.1	Ag_3Sn + ζAg
D2	11.3	0.7	9.6	13.4	Ag_3Sn + ζAg

other hand, the mean thicknesses for samples A2 and B2 are clearly larger than those for samples A0, A1, B0, and B1. This can be ascribed to the fact that Ag_3Sn IMC formed during the early bonding stage had been converted into ζAg IMC, which thus increased the total thickness of the Ag–Sn IMCs during the late bonding stage. In addition, the ratios of the maximum to the mean thicknesses of the Ag–Sn IMCs for samples A0 and B0 are equal or close to 2, whereas those for samples A1, A2, B1, and B2 are somewhat lower than 2.

The mean thicknesses of the Ni_3Sn_4 IMC formed on the IGBT sides, also measured by use of the image analysis method, were both approximately 4.0 μm for samples A0 and B0, and all in the range 2.0 μm–2.5 μm for samples A1, A2, B1, and B2.

Dummy Si Chips with Thickened Ni/Ag Metallization

As shown in Figs. 6 and 7, if dummy Si chips with 1/6 μm thick Ni/Ag metallization were bonded to Ag foil plated with 2.7 μm thick Sn, the Ni barrier layer beneath the Ag layer was intact and some residual Ag was retained on the chip side of both samples C1 and C2. For sample C1 bonded at 250°C for 40 min, the joint mainly consisted of relatively coarse Ag_3Sn grains plus finer ζAg grains which were similar to each other on both the chip side and the Ag foil side (Fig. 7a). For sample C2 bonded at 250°C for 640 min, the joint consisted of ζAg grains only which were also similar to each other on both the chip side and the Ag foil side (Fig. 7b).

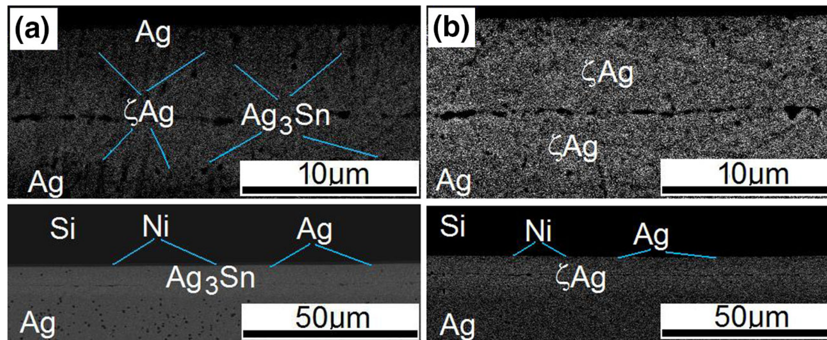

Fig. 6. SEM images of polished cross sections of dummy Si chips with thickened Ni/Ag metallization on 100 μm thick Ag foil electroplated with 2.7 μm thick Sn at 250°C and 2 MPa: (a) sample C1, 40 min; (b) sample C2, 640 min.

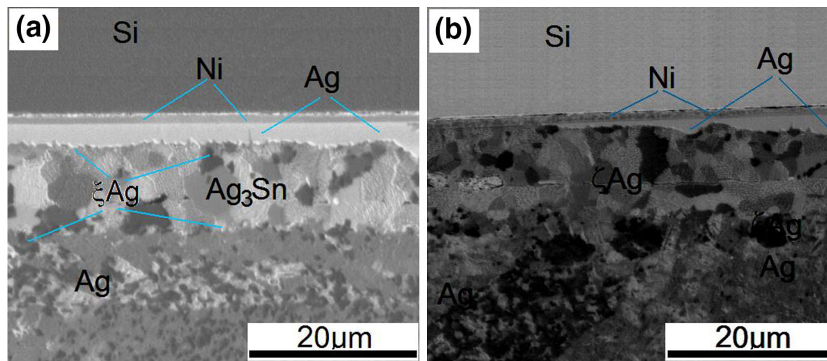

Fig. 7. FIB images of polished cross sections of dummy Si chips with thickened Ni/Ag metallization on 100 μm thick Ag foil electroplated with 2.7 μm thick Sn at 250°C and 2 MPa: (a) sample C1, 40 min; (b) sample C2, 640 min.

As can be seen from Fig. 8, if the dummy Si chips with 1/6 μm thick Ni/Ag metallization were bonded to Ag foil plated with 6.8 μm thick Sn, the Ni barrier layer beneath the Ag layer was locally attacked by Sn to produce Ni_3Sn_4 IMC on the chip side. This reveals that the liquid Sn layers in the bonding areas of these samples were somewhat thicker than those in the bonding areas of samples C1 and C2 during the initial bonding stage. After the Ag layers on the Si chips had been consumed, residual Sn migrated through the grain boundaries and/or molten channels between the Ag_3Sn crystals formed during the early stage and reacted with the Ni barrier layers. For sample D1 bonded at 250°C for 40 min, the joint consisted of Ag_3Sn IMC plus local Ni_3Sn_4 IMC on the chip side, and major Ag_3Sn IMC plus minor ζAg IMC on the Ag foil side. For sample D2 bonded at 250°C for 640 min, the joint also consisted of Ag_3Sn IMC plus local Ni_3Sn_4 IMC on the chip side. However, on the Ag foil side, the joint consisted of major ζAg IMC plus minor Ag_3Sn IMC. Note that for samples D1 and D2 Ag–Sn IMCs could be observed on both the Si chip side and the Ag foil side; this is somewhat different from samples A1 and A2 for which Ag–Sn IMCs were observed on the Ag foil side only (Fig. 5).

As listed in Table II, the total thickness of the Ag–Sn IMCs formed in sample C2 is larger than that of the Ag–Sn IMCs formed in sample C1. This can be related to the change of the Ag_3Sn IMC formed during the early bonding stage into ζAg IMC during the late bonding stage. However, the total thickness of the Ag–Sn IMCs formed in sample D2 is similar to that of the Ag–Sn IMCs formed in sample D1. This may be because different amounts of liquid Sn had partially been squeezed from the bonding areas of samples D1 and D2 during the early bonding stage.

Comparison of the total thicknesses of the Ag–Sn IMCs formed in samples C1, C2, D1, and D2 with those formed in samples A1, A2, B1, and B2 reveals that the former values are all more than twice as large as the latter values. This indicates that less Sn was available to react with Ag in samples A1, A2, B1, and B2 than in samples C1, C2, D1, and D2. Therefore, the rate of reaction of the liquid Sn with the Ni barrier layer was probably higher than that of the liquid Sn with the Ag in the samples of the real IGTBs bonded to Ag foil.

In addition, the separate thicknesses of Ag_3Sn and ζAg IMCs formed in sample C1 will be used to extract the diffusivities of Ag and Sn in Ag (presented below). They can be separated from the total thicknesses listed in Table II by use of the FIB image shown in Fig. 7a. Values of 5.9 μm and 2.0 μm were estimated for the thicknesses of the

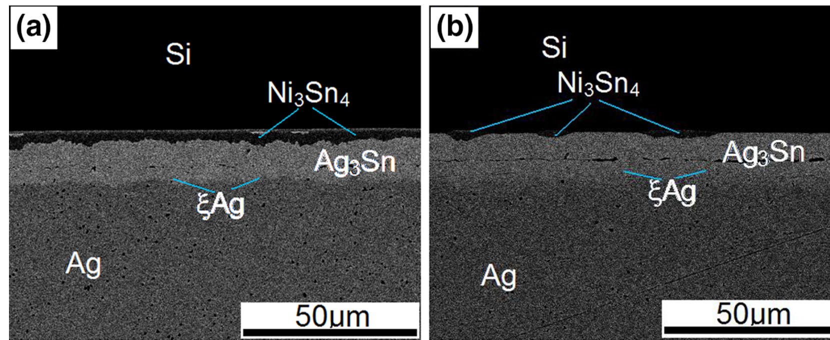

Fig. 8. SEM images of polished cross sections of the samples of dummy Si chips with thickened Ni/Ag metallization on 100 μm thick Ag foil electroplated with 6.8 μm thick Sn at 250°C and 2 MPa: (a) sample D1, 40 min; (b) sample D2, 640 min.

Ag_3Sn IMC in the middle and the ζAg IMC on both the dummy Si chip side and the Ag foil side, respectively.

DISCUSSION

Interfacial Microstructure

As can be seen from Fig. 1, the solubility of Ag in liquid Sn at 250°C is approximately 5 at.%, and the amount of Ag dissolved into the liquid Sn during the bonding process should be negligible. Therefore, observation of Ag–Sn IMCs on the Ag foil side only for all the samples with real IGBTs attached cannot be attributed to dissolution of 0.7 μm Ag into the 2.7 μm (and even 6.8 μm thick) liquid Sn during the early bonding stage. It is more likely this is related to rapid coarsening of relatively small Ag_3Sn scallops and can be explained as follows.

The effect of initial dissolution of Ag and nucleation of Ag_3Sn may be ignored, because these processes were extremely rapid. In agreement with our previous work on the Ag/Sn/Ag TLP system,[5] until the liquid Sn was consumed, only Ag_3Sn scallops were formed between the Sn and Ag. Evolution of the average thickness of the Ag_3Sn layer with bonding time can be described by use of Eq. 1[5]:

$$x_{Ag_3Sn} = 3.573 \times 10^3 \exp\left(-\frac{37.17 \pm 18.87}{RT}\right) t^{1/3},$$
$$0 \le x_{Ag_3Sn} \le x_{Ag_3Sn,max}, \quad (1)$$

where x_{Ag_3Sn}, is the average thickness of the Ag_3Sn layer in μm, t is time in seconds, R is the universal gas constant, T is the absolute temperature, and $x_{Ag_3Sn,max}$ is maximum thickness of the Ag_3Sn layer, during formation of which the Sn interlay is consumed in accordance with the reaction (Eq. 2):

$$Sn + 3Ag \rightarrow Ag_3Sn \quad (2)$$

If Eqs. 1 and 2 are extended to relatively low bonding temperature, the melting point of the eutectic Sn–3.5Ag alloy, 221°C, they may be used to calculate the growth of the Ag_3Sn IMC and consumption of the Ag base metal layers and the Sn interlayer during the early bonding stage. The results calculated for bonding temperatures of 221°C and 250°C are shown in Fig. 9. The densities of Sn, Ag, and Ag_3Sn used during the calculation are listed in Table III. It can be seen that a layer of Ag 0.7 μm thick reacting with ~0.35 μm thick Sn (~0.7 μm thick Sn in total for two sides) produces ~1 μm thick Ag_3Sn IMC on one side of the Ag/Sn/Ag TLP sample. This takes only 2 min and 0.4 min at bonding temperatures of 221°C and 250°C, respectively. Therefore, on the basis of the temperature profile shown in Fig. 4b, bonding times for the Sn interlayer to stay above the melting point should have been sufficient to consume the 0.7 μm thick Ag metallization on all the real IGBTs of our TLP samples, even for a bonding time of 0 min at 250°C.

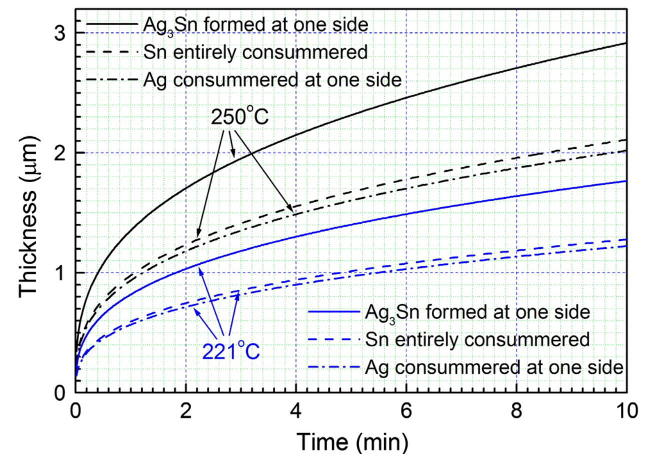

Fig. 9. Growth of the Ag_3Sn IMC and consumption of the Ag base metal layers and the Sn interlayer in Ag/Sn/Ag TLP samples during the early stage of bonding for bonding temperatures of 221°C and 250°C, calculated by use of Eqs. 1 and 2.

As also reported in our previous paper,[5] growth of the Ag_3Sn IMC between liquid Sn and solid Ag could be well explained on the basis of grain boundary and/or molten channel-controlled growth. When the 0.7 μm thick Ag on one IGBT was consumed, liquid Sn remaining would thus penetrate the grain

Table III. The values used in this numerical simulation for the molar fraction of Sn, the densities and molar volumes of the different phases and interfaces in Ag/Sn/Ag TLP joints, calculated on the basis of the binary Ag–Sn phase diagram and the lattice cell parameters reported in Refs. 24–31

Phase		Ag	ζAg	ζAg	Ag_3Sn	
Interface	**Ag**	**Ag/ζAg**	**Ag/ζAg**	**ζAg/Ag_3Sn**	**ζAg/Ag_3Sn**	**Sn**
Molar fraction of Sn	0	0.085	0.103	0.173	0.250	1
Density (g/cm^3)	10.49	10.39	10.31	10.11	9.92	7.36
Molar volume (cm^3/mol)	10.28	10.47	10.56	10.86	11.14	16.12

boundaries between the Ag_3Sn IMC crystals to further rapidly attack and react with the Ni layer beneath the original Ag metallization, forming the Ni_3Sn_4 IMC on the IGBT side. As the amount of liquid Sn decreased, the Ag_3Sn IMC crystals or scallops formed on the two sides gradually came into contact with each other. Relatively small Ag_3Sn IMC crystals or scallops formed on the two sides tended to coalesce into relatively large Ag_3Sn scallops as they formed and grew. This is probably why the Ag–Sn IMCs were observed on the Ag foil side only for all the samples with attached real IGBTs (Fig. 4). For samples with attached dummy Si chips and thickened Ag metallization, the Ag_3Sn scallops formed on the two sides were already too large to coarsen further before coming into contact with each other. Therefore, for these samples, the Ag_3Sn scallops were observed on both the chip side and the Ag foil side (Figs. 5 and 7).

Given that the average thicknesses of the Ag–Sn IMCs in samples A0, A1, B0, and B1 were all approximately 2 μm (Table II), it can be estimated by use of Eq. 2 and Fig. 9 that the average thickness of the Ag consumed on the Ag foil side of these samples was also ~0.7 μm. The rate of the reaction between the liquid Sn and the Ag foil might be the same as or lower than that between the liquid Sn and the Ag metallization on the IGBT. Nevertheless, only an ~0.7 μm thick Sn interlayer was consumed by ~0.7 μm (~1.4 μm in total for the two sides) thick Ag on both the IGBT and Ag foil sides to form the Ag_3Sn IMC (Fig. 9). More of the Sn interlayer, i.e. ~2.0 μm thick Sn if the Sn interlayer was 2.7 μm thick, was consumed by the Ni layer to produce the Ni_3Sn_4 IMC on the IGBT side of each of these samples. According to the reaction (Eq. 3):

$$4Sn + 3Ni \rightarrow Ni_3Sn_4. \quad (3)$$

and with densities of 7.36 g/cm^3, 8.91 g/cm^3, and 8.65 g/cm^3 for Sn, Ni, and Ni_3Sn_4, consumption of 2.0 μm thick Sn would require 0.6 μm thick Ni and produce 2.3 μm thick Ni_3Sn_4 IMC. These values are in good agreement with the thickness of 0.8 μm for the Ni layer on the IGBTs and thicknesses in the range 2.0–2.5 μm for the Ni_3Sn_4 IMC formed in samples A1, A2, B1, and B2. The relatively thicker ~4.0 μm thick Ni_3Sn_4 IMC formed in samples A0 and B0 may be attributed to the existence of boundaries between the Ni_3Sn_4 IMC grains. With increasing the bonding time, the Ni_3Sn_4 IMC grains ripened and the grain boundaries migrated and developed into a chain of voids along the interface between the Ni_3Sn_4 IMC and the Ag–Sn IMCs, as shown in Fig. 5. In addition, as aforementioned, the microstructure and mean thicknesses of both the Ag–Sn IMCs and the Ni_3Sn_4 IMC in samples A0 to A2 were similar to those in the corresponding samples B0 to B2. This reveals that approximately 4 μm thick liquid Sn had probably been squeezed out of the bonding areas during the preparation of samples B0 to B2.

The solubility of Ni in liquid Sn is even lower than that of Ag at a same temperature.[19] The Ni_3Sn_4 IMC on the IGBT side should hence have been formed by solid–liquid interfacial reaction. The solid–liquid interfacial reaction between Ni and liquid Sn to produce Ni_3Sn_4 IMC has also been reported to be grain boundary and/or molten channel-controlled.[20,21] A trace of Sn mixed with the Ni_3Sn_4 IMC was observed for the sample formed at 250°C for 0 min, because it was trapped within the grain boundaries and/or molten channels. The start of the reaction of the solid Ni with the liquid Sn was later than that between the solid Ag, on both the IGBT and Ag foil sides, with the liquid Sn. However, reaction of Ni with Sn still consumed much more of the liquid Sn than reaction of Ag with Sn. This reveals that the interfacial reaction between the liquid Sn and the Ni layer was extremely rapid compared with that between the liquid Sn and both the Ag metallization and the Ag foil. This result is not in agreement with the kinetic constants for the growth of Ni_3Sn_4 and Ag_3Sn scallops reported in the literature.[5,20,21] This may be associated with the application of pressure in our bonding process, but further investigation is needed to provide true understanding.

Suitable Thicknesses of Ag and Sn Layers for Die Attachment

To achieve improved reliability, the processed Ag/Sn/Ag TLP joints used for power die attachment should contain neither remaining Sn nor any Ni_3Sn_4 IMC in contact with the Ag_3Sn IMC. This is because remaining Sn with its low melting point has relatively poor mechanical strength and creep

resistance. In particular, when the operating temperature is close to and/or above the melting point, the mechanical strength of the joint will be reduced substantially or even lost. On the other hand, the ripening process of the Ni_3Sn_4 grains would lead to the formation and growth of a chain of voids between the Ag_3Sn and Ni_3Sn_4 IMCs, as shown in Fig. 5, during the extended bonding stage and/or during high temperature application. These would not only lead to deterioration of the thermal performance of the joints but also act as the sites for nucleation and growth of cracks. Therefore, the presence of both remaining Sn and Ni_3Sn_4 IMC in contact with the Ag_3Sn IMC in the Ag/Sn/Ag TLP joints would reduce their reliability.

As already mentioned, the thicknesses of the Ag_3Sn IMC formed and of the Ag layers required to consume Sn interlayers of different thickness can be simply calculated by use of Eqs. 1 and 2. However, because of the grain boundary and/or molten channel-controlled growth of the Ag_3Sn IMC between the liquid Sn and the solid Ag and the non-flat interfaces between the formed Ag_3Sn IMC and the residual Ag, local Ag might be consumed in greater amounts and more quickly than the rest of the Ag layer in reaction with liquid Sn to produce Ag_3Sn IMC during the bonding process. As a result, the Ag layers to be deposited on the power die and substrate sides as base metal layers should be thicker than those calculated on the basis of Eq. 2. Otherwise, once the local Ag layer is consumed, Sn atoms will be rapidly delivered through the grain boundaries and/or molten channels between the Ag_3Sn crystals to attack the Ni layer and produce Ni_3Sn_4 IMC. This is verified by formation of local Ni_3Sn_4 IMC in samples D1 and D2, as shown in Fig. 8. Although the original thickness of the Sn interlayer of both samples was 6.8 μm, the actual thickness of the Sn interlayer in the bonding areas should be thinner than 6 μm, which can consume approximately 6 μm thick Ag on both the dummy Si chip side and the Ag foil side (Fig. 9). This is because the Sn was observed to be partially squeezed from the bonding areas of both samples during the bonding process, as mentioned above.

Again as reported in our previous paper,[5] before the Ag_3Sn grains formed on the two sides of the Ag/Sn/Ag samples came into contact with each other, the ratios of the maximum to the mean values for the Ag_3Sn IMC thicknesses in the different samples were in the range 1.9–2.6. Similar ratios of the maximum to the mean values for the Ag_3Sn IMC thicknesses were also observed in the samples A0 and B0. These values are in good agreement with steady-state particle coarsening theories, which predict an upper limit on particle size approximately 2–2.5 times the mean particle size.[20,22] We may, therefore, consider an increase by a factor of at least two in the thickness of the Ag layer needed to consume the Sn interlayer by production of the Ag_3Sn IMC. This may prevent attack by liquid Sn of the Ni barrier layer beneath the Ag layer during the TLP bonding process. In such circumstances, the thicknesses of the Ag layers which must be deposited on both the power die and the supporting substrate should be at least twice the entire thickness of the Sn interlayer in the middle. For example, if the total thickness of the Sn interlayer is 2 μm, Ag layers at least 4 μm thick should be deposited on both the power die and the supporting substrate.

Given the difficulty of depositing Ag layers thicker than 10 μm on semiconductor power devices, the Sn interlayers used for producing the Ag/Sn/Ag TL joints should usually be thinner than 5 μm. A more suitable thickness of the Sn interlayer may be 2–3 μm, in combination with Ag layers 4–6 μm thick, which are easy to deposit on both the semiconductor power die and the supporting substrate. As demonstrated by the results shown in Figs. 6 and 7, such a combination of thicknesses of the Sn interlayer and the Ag base metal layers can indeed be used to produce Ag/Sn/Ag TLP joints of good quality.

Diffusivities of Ag and Sn in ξAg IMC

Before the remaining Sn was consumed, no ζAg IMC was detected in any of the Ag/Sg/Ag samples reported previously.[5] We may, hence, assume that the ζAg IMC started to form and grow at the time when the Ag_3Sn IMC layer in the samples, formed in accordance with Eq. 2, had already reached its maximum thickness. Also, we may ignore the timescale for nucleation of the ζAg crystals and assume that thickening of the ζAg layer is diffusion-controlled at the expense of the Ag_3Sn layer formed previously. Furthermore, we may assume that diffusion of Ag and Sn in both the ζAg IMC and Ag phases is governed by the Darken interdiffusion coefficient[23]:

$$D(N_{Sn}) = N_{Sn} D_{Sn} + (1 - N_{Sn}) D_{Ag}, \qquad (4)$$

where $D(N_{Sn})$ is the Darken interdiffusion coefficient, N_{Sn} is molar fraction of Sn, D_{Sn} and D_{Ag} are the diffusivities of Sn and Ag both in the ζAg IMC or in both the Ag phases. On the basis of these assumptions, the thicknesses of the Ag_3Sn and ζAg IMCs in samples C1 and C2 can be used to obtain the diffusivities of Ag and Sn in the ζAg IMC.

First, using the kinetic constants for Ag_3Sn growth reported previously,[5] and if the effect of initial dissolution of Ag and nucleation of Ag_3Sn are ignored, evolution of the average thickness of the Ag_3Sn layer with bonding time can be described by use of Eq. 1. Equation 1 in combination with Eq. 2 can be used to calculate the time, t_0, when the Sn interlayer was consumed, the growth of the Ag_3Sn IMC, and consumption of the Ag base metal layers and the Sn interlayer during the early bonding stage.

Growth of the ζAg IMC at the expense of the Ag_3Sn IMC formed previously and subsequent

evolution with bonding time of the ζAg IMC can then be simulated by use of a fixed-grid numerical method described elsewhere.[24,25] Essentially, this numerical method can be used to obtain the distribution and evolution with bonding time of the molar fractions, N_{Sn}, across the Ag/Sn/Ag TLP joints, on the basis of Fick's diffusion law, as illustrated schematically in Fig. 10.

The governing equations are:

$$\frac{\partial[N_{\mathrm{Sn}}(x,t)/V(x,t)]}{\partial t}=\frac{\partial}{\partial x}\left[D(N_{\mathrm{Sn}})\frac{\partial[N_{\mathrm{Sn}}(x,t)/V(x,t)]}{\partial x}\right],\quad S_{I-1}(t)<x<S_I(t),\ I=1,\ldots,5 \tag{5}$$

$$D_I^-(N_{\mathrm{Sn}})\left.\frac{\partial[N_{\mathrm{Sn}}(x,t)/V(x,t)]}{\partial x}\right|_{x=S_I(t)^-}-D_I^+(N_{\mathrm{Sn}})\left.\frac{\partial[N_{\mathrm{Sn}}(x,t)/V(x,t)]}{\partial x}\right|_{x=S_I(t)^+}=\left[N_I^-/V_I^- - N_I^+/V_I^+\right]\frac{\partial S_I(t)}{\partial t},\quad x=S_I(t),\quad I=1,\ldots,4 \tag{6}$$

These are subject to the boundary conditions:

$$\frac{\partial[N_{\mathrm{Sn}}(x,t)/V(x,t)]}{\partial x}=0,\quad x=S_0(t)=L_0 \tag{7a}$$

$$\frac{\partial[N_{\mathrm{Sn}}(x,t)/V(x,t)]}{\partial x}=0,\quad x=S_5(t)=L_1. \tag{7b}$$

And the initial conditions can be given as:

$$N_{\mathrm{Sn}}(x,t)/V(x,t)=N_{\mathrm{Sn}}(x,t_0)/V(x,t_0),\quad S_0(t_0)\le x\le S_5(t_0), \tag{8}$$

where x is position coordinate, V is molar volume, L_0 and L_1 are two boundaries of one TLP joint, S_I ($I = 1,\ldots,4$) are moving interfaces of phases, and superscripts − and + stand for the left and right sides of the moving interfaces.

In this work, the values used in the simulation for the molar fraction of Sn, density, and molar volume of the different phases and interfaces in the Ag/Sn/Ag TLP joints are listed in Table III. They were calculated on the basis of the binary Ag–Sn phase diagram and the lattice cell parameters reported in Refs. 18,26–32. Inside each of the phases, the density and molar volume were assumed to be linearly related to the molar fraction of Sn. The diffusivities of Ag and Sn in Ag estimated from the Arrhenius-type plots in Ref. 21 were taken as known values for calculation of the Darken interdiffusion coefficient of the Ag phase. The stoichiometric width of the Ag_3Sn IMC is extremely narrow and was taken as zero; hence diffusion of atoms inside the Ag_3Sn layer may be ignored. With this assumption, the interdiffusion coefficients of the Ag_3Sn layer can be taken as any value.

Data fitting of the measured thicknesses of the Ag_3Sn and ζAg layers in samples C1 and C2 with those simulated using the numerical method to solve Eqs. 5–8 was used to determine the diffusivities of Ag and Sn in ζAg. For each simulation, at time t_0, there are Ag_3Sn and Ag phases only in the Ag/Sn/Ag TLP joint, and their molar fractions were set as 0.25 and 0, respectively. During the simulation, the $D(N_{Sn})$ and V dependent on the N_{Sn} were updated with an iteration method, and convergence of the calculation was verified by a relative error less than 1.0×10^{-4}.

The best fits of the measured thicknesses of the Ag_3Sn and ξAg layers in samples C1 and C2 to those simulated by use of the numerical method are plotted in Fig. 11. It can be seen that the simulated Ag_3Sn/ξAg and ξAg/Ag interfaces are in good agreement with the experimental solid points. The diffusivities of Ag and Sn in ζAg IMC at 250°C, determined by data fitting, are 5.73×10^{-16} m²/s

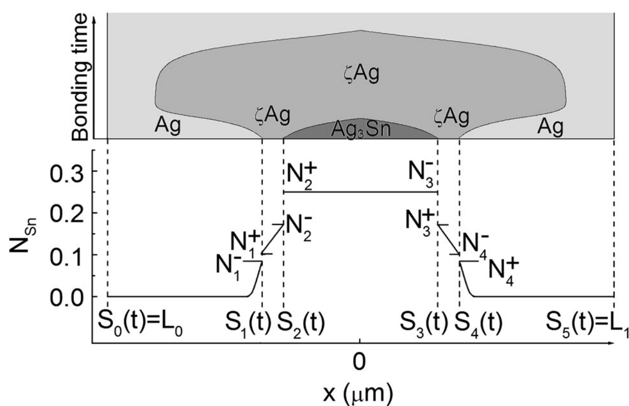

Fig. 10. Schematic illustration of the one-dimensional distribution of the molar fraction N_{Sn} across one Ag/Sn/Ag TLP joint at time t_0 immediately after the Sn interlayer has been fully consumed.

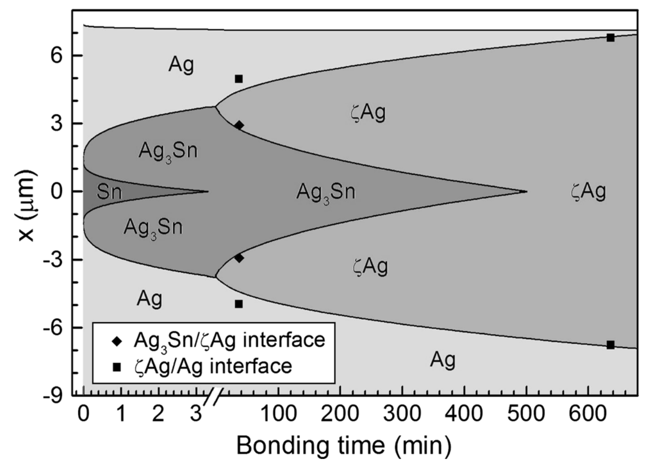

Fig. 11. Data fitting of the measured thicknesses of the Ag_3Sn and ξAg layers in samples C1 and C2 (solid points) with those simulated by using the numerical method to solve Eqs. 1–7a, b.

Table IV. Diffusivities of Ag and Sn in Ag calculated from the Arrhenius-type plots in Ref. 21 and those in ζAg IMC extracted in this study

	Diffusivity at 250°C (m^2/s)	Refs.
Ag in Ag	3.72×10^{-23}	Calculated from data in Ref. 21
Sn in Ag	1.10×10^{-21}	Calculated from data in Ref. 21
Ag in ζAg	5.73×10^{-16}	Extracted in this study
Sn in ζAg	7.92×10^{-17}	Extracted in this study

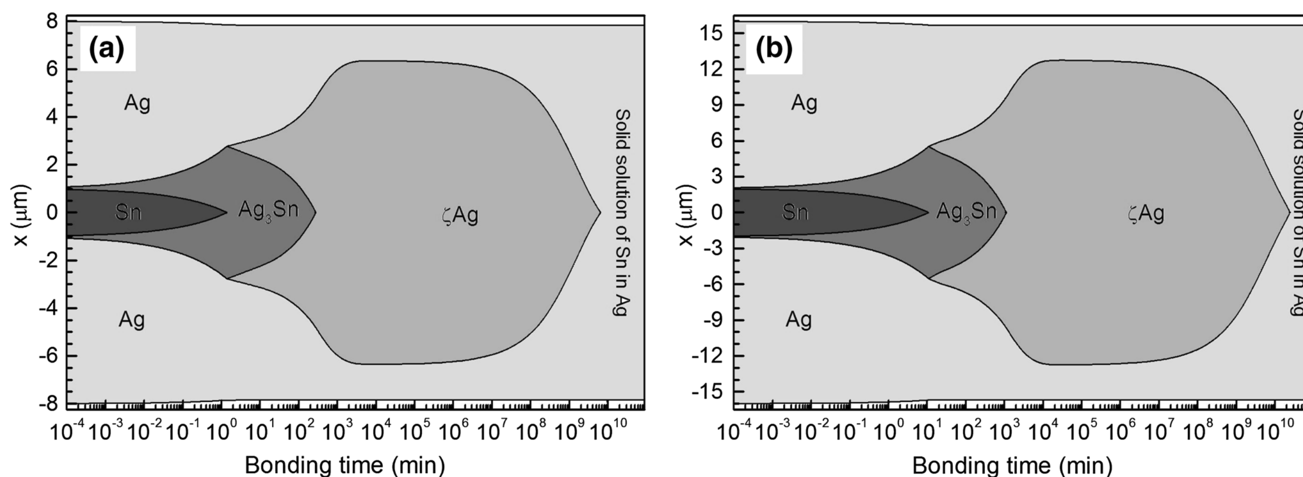

Fig. 12. Simulated growth and evolution of phases in the Ag/Sn/Ag TLP joints during the extended bonding process at 250°C: (a) 2 μm thick Sn interlayer sandwiched between two layers of 7 μm thick Ag base metal; and (b) 4 μm thick Sn interlayer sandwiched between two layers of 14 μm thick Ag base metal.

and 7.92×10^{-17} m^2/s, as listed in Table IV. They are approximately seven and three orders of magnitude higher, respectively, than those of Ag and Sn in Ag at the same temperature (250°C). On the other hand, they are slightly higher than the volume diffusivities of Ag and Sn in Ag_3Sn IMC, but significantly lower (four to six orders of magnitude lower) than the grain-boundary diffusivities of Ag and Sn in Ag_3Sn IMC reported in Ref. 33.

Evolution of Phases During the Extended Bonding Process

With the extracted diffusivities of Ag and Sn in ζAg IMC at 250°C, evolution of the phases in two Ag/Sn/Ag TLP joints during the extended bonding process were simulated by use of the same numerical method to solve Eqs. 1 and 5–8. One of the joints was assumed to produce using a 2 μm thick Sn interlayer sandwiched between two layers of 7 μm thick Ag base metal. The other one was assumed to produce using a 4 μm thick Sn interlayer sandwiched between two layers of 14 μm thick Ag base metal. The combined thicknesses of the Sn interlayer and the Ag base metal layers in both simulated joints were selected to achieve final joints consisting of a solid solution of Sn in Ag with an Sn molar fraction of 0.0835, which is slightly lower than the equilibrium Sn molar fraction of 0.085 at the interface of Ag in contact with ξAg IMC.[18]

The simulated results are shown in Fig. 12, in which the horizontal axes are logarithmic. It can be seen that the timescales for consumption of the Sn interlayers to produce Ag_3Sn IMC are two orders of magnitude shorter than those for consumption of the Ag_3Sn IMC layers formed previously to produce ξAg IMC. Given that initial dissolution of Ag in liquid Sn and nucleation of Ag_3Sn crystals are even more rapid, the effect on the extracted diffusivities of Ag and Sn in ζAg IMC of ignoring them during the early bonding stage should be negligible.

It is apparent that the ξAg IMC will continue to grow after the Ag_3Sn IMC is consumed. This can be attributed to net diffusion of Sn atoms toward the Ag/ξAg interfaces from the part of the ξAg IMC in the middle of the joints formed during the earlier stage with higher molar fractions of Sn. The bonding times for consuming the Ag_3Sn IMC to produce the ξAg IMC and for consuming the ξAg IMC to form the final solid solution of Sn in Ag are 280 min and 6.5×10^9 min in Fig. 12a, and 1120 min and 2.60×10^{10} min in Fig. 12b. With these timescales in mind, it is more realistic to process Ag/Sn/Ag TLP joints consisting of major Ag_3Sn IMC plus minor ξAg IMC and residual Ag for power die attachment. Under the application environments, temperatures

can be below the 250°C used in the simulation, and the rates of evolution of the phases in this case would be much slower than those shown in Fig. 12. Therefore, the Ag/Sn/Ag TLP joints can be expected to consist of ξAg IMC plus residual Ag during most of the service lifetime if Ag/Sn/Ag TLP joints are used for power die attachment.

If the thicknesses of the Ag base metal on both the power die and supporting substrate sides are just 2–2.5 times the thickness of the entire Sn interlayer, the processed Ag/Sn/Ag TLP joints can still be expected to consist of major ξAg IMC plus minor residual Ag during most of the service lifetime. This is because, on the one hand, at the application temperatures used, the rates of evolution of phases in the TLP joints should be much slower than those shown in Fig. 12. On the other hand, even if the Ag base metal layers are consumed, any possible further solid/solid interfacial reaction between ξAg IMC and Ni barrier layer should also be very slow. This is because no ternary Sn-Ag-Ni IMC is present in the Sn-Ag-Ni system,[19] and the supply of Sn from the ξAg IMC to the Ni barrier layer for producing new Ni-Sn IMC is limited.

CONCLUSIONS

From the above results and discussion of the Ag/Sn/Ag TLP joints used for power die attachment, the following conclusions can be drawn:

1 The thickness of the Ag base metal layers on both the power die and the supporting substrate should be at least twice the average thickness required to consume the Sn interlayer for producing Ag_3Sn IMC. Otherwise, the Ni barrier layer beneath the original Ag layer will be locally attacked by liquid Sn to form the Ni_3Sn_4 IMC, which may lead to formation and growth of a chain of voids along the interface between the Ni_3Sn_4 and Ag–Sn IMCs during the extended bonding process and/or in service.
2 A thickness of 2–3 μm for the Sn interlayer in combination with a thickness of 4–6 μm for the Ag base metal layers deposited on both the semiconductor power die and the supporting substrate will be suitable for producing the Ag/Sn/Ag TLP joints used for power die attachment. That this combination of Sn interlayer and Ag base metal layers produces high-quality of Ag/Sn/Ag TLP joints is demonstrated by the results shown in Figs. 6 and 7.
3 The diffusivities of Ag and Sn in ζAg IMC at 250°C, determined by the data fitting of the measured thicknesses of the Ag_3Sn IMC and ξAg IMC layers to results simulated by use of a numerical method are 5.73×10^{-16} m^2/s and 7.92×10^{-17} m^2/s, respectively. They are slightly higher than the volume diffusivities of Ag and Sn in Ag_3Sn IMC, but four to six orders of magnitude lower than the grain-boundary diffusivities of Ag and Sn in Ag_3Sn IMC reported in the literature.
4 Simulated results for evolution of the phases in Ag/Sn/Ag TLP joints indicate that it is more realistic, for power die attachment, to process Ag/Sn/Ag TLP joints consisting of major Ag_3Sn IMC plus minor ξAg IMC and residual Ag. The Ag/Sn/Ag TLP joints can be expected to consist of major ξAg IMC plus residual Ag during most of the service lifetime if Ag/Sn/Ag TLP joints are used for power die attachment.

ACKNOWLEDGEMENTS

This research was supported by the UK Engineering and Physical Science Research Council as part of the Innovative Electronic Manufacturing Research Centre (IeMRC) (grant number EP/H03014X/1) and the European Commission through the Seventh Research Framework Programme, CleanSky "Systems for Green Operations".

OPEN ACCESS

This article is distributed under the terms of the Creative Commons Attribution License which permits any use, distribution, and reproduction in any medium, provided the original author(s) and the source are credited.

REFERENCES

1. L. Bernstein, *J. Electrochem. Soc.* 113, 1282 (1966).
2. C.C. Lee and C.Y. Wang, *Thin Solid Films* 208, 202 (1992).
3. G.S. Matijasevic, C.C. Lee, and C.Y. Wang, *Thin Solid Films* 223, 276 (1993).
4. G. Humpston and D.M. Jacobson, *Principles of Soldering* (Materials Park: ASM International, 2004), pp. 230–235.
5. J.F. Li, P.A. Agyakwa, and C.M. Johnson, *Acta Mater.* 58, 3429 (2010).
6. J.F. Li, P.A. Agyakwa, and C.M. Johnson, *Acta Mater.* 59, 1198 (2011).
7. D.E. Crees, G. Humpston, D.M. Jacobson, and D. Newcombe, *GEC J. Res.* 6, 71 (1988).
8. T.B. Wang, Z.Z. Shen, R.Q. Ye, X.M. Xie, F. Stubhan, and J. Freytag, *J. Electron. Mater.* 29, 443 (2000).
9. F. Bartels, J.W. Morris, G. Dalke, and W. Gust, *J. Electron. Mater.* 23, 787 (1994).
10. E. Lugscheider, K. Bobzin, and M.K. Lake, *Surf. Coat. Technol.* 142–144, 813 (2001).
11. N.S. Bosco and F.W. Zok, *Acta Mater.* 53, 2019 (2005).
12. E. Lugscheider, K. Bobzin, M. Maes, S. Ferrara, and A. Erdle, *Surf. Coat. Technol.* 200, 444 (2005).
13. S. Sommadossi, W. Gust, and E.J. Mittemeijer, *Mater. Chem. Phys.* 77, 924 (2002).
14. P.K. Khanna, G. Dalke, and W. Gust, *Z. Metallkd.* 90, 722 (1999).
15. N. Quitoriano, W.S. Wong, L. Tsakalakos, Y. Cho, and T. Sands, *J. Electron. Mater.* 30, 1471 (2001).
16. T. Studnitzky and R. Schmid-Fetzer, *J. Electron. Mater.* 32, 70 (2003).
17. K. Guth, N. Oeschler, L. Bower, R. Speckels, G. Strotman, N. Heuck, S. Krasel, A. Ciliox, in *Proceedings of 7th International Conference on Integrated Power Electronics Systems*, 6–8 March 2012, Nuremberg, Germany, pp. 380–384.
18. "Binary Ag–Sn phase diagram," Facility for the Analysis of Chemical Thermodynamics (FACT). http://www.crct.polymtl.ca/FACT/phase_diagram.php?file=Ag–Sn.jpg&dir=SGTE.
19. H.F. Hsu and S.W. Chen, *Acta Mater.* 52, 2541 (2004).
20. G. Ghosh, *J. Appl. Phys.* 88, 6887 (2000).
21. G. Ghosh, *Acta Mater.* 49, 2609 (2001).
22. V. Tikare and J.D. Cawley, *Acta Mater.* 46, 1333 (1998).

23. Z. Mei, A.J. Sunwoo, and J.W. Morris Jr, *Metall. Trans.* A23, 857 (1992).
24. J.F. Li, P.A. Agyakwa, and C.M. Johnson, *J. Mater. Sci.* 45, 2340 (2010).
25. J.F. Li, P.A. Agyakwa, and C.M. Johnson, *Intermetallics* 40, 50 (2013).
26. H.W. King and T.B. Massalski, *Philos. Mag.* 6, 669 (1961).
27. W. Klement Jr, *Trans Metall Soc AIME* 233, 1182 (1965).
28. R.H. Kane, B.C. Giessen, and N.J. Grant, *Acta Metall.* 14, 605 (1966).
29. C.W. Fairhurst and J.B. Cohen, *Acta Crystallogr.* B28, 371 (1972).
30. S. Barat and J.K. Mukherjee, *Indian J. Technol.* 13, 510 (1975).
31. Y. Ning and X. Zhou, *J. Alloys Compd.* 182, 131 (1992).
32. E. Roennebro, J. Yin, A. Kitano, M. Wada, and T. Sakai, *Solid State Ion.* 176, 2749 (2005).
33. T. Okabe, R.F. Hochman, and M.E. Mclain, *J. Biomed. Res.* 8, 381 (1974).